Electronic Supplementary Material (ESI) for Soft Matter.

Supplemental Material

Mechanics and microstructure of blood plasma clots in shear driven rupture

Ranjini K. Ramanujam[a,*], Konstantinos Garyfallogiannis[b,*], Rustem I. Litvinov[c], John L. Bassani[b], John W. Weisel[c], Prashant K. Purohit[b#], Valerie Tutwiler[a#]

[a] Department of Biomedical Engineering, Rutgers University, Piscataway, NJ, USA
[b] Department of Mechanical Engineering and Applied Mechanics, University of Pennsylvania, Philadelphia, PA, USA
[c] Department of Cell and Developmental Biology, University of Pennsylvania, Philadelphia, PA, USA
*Co-first authors
#Co-corresponding authors

Calculating Π from experiments

Evaluation of $\tilde{G}_c$ requires knowledge of the potential energy Π evaluated at $\Delta = \Delta_c$. Π is nothing but the energy stored in elastic deformations of the fibers, which is the area below a force-displacement curve in displacement-controlled experiments. In Tutwiler et al. [11] and Garyfallogiannis et al. [10] the force displacement curve is very close to linear and hence a linear fit of the data of the following form is used:

$$F(\Delta) = \frac{F_{max}}{\Delta_c}\Delta \qquad \text{(S1)}$$

with Δ the overall displacement and F_{max} the peak force at $\Delta = \Delta_c$. Knowing the relation that relates force to displacement, the integration to obtain the stored energy is straightforward. However, in shear the force-displacement curves are strongly non-linear, and a linear fit as in (S1) is no longer appropriate. A quadratic fit of the form below is selected:

$$F(\Delta) = k_1\Delta + k_2\Delta^2 \qquad \text{(S2)},$$

with $k_1$and k_2 obtained by minimizing the square error of (S2) with the experimental data points. Comparison of the linear and quadratic fit for the shear experiments with 2.9 mg/ml fibrin(ogen) concentration for four crack lengths is shown in Fig. S1. The quadratic fit (red) captures the data (blue) far better than the linear fit (green). Then, the values of Π are used to compute the energy release rate by the method suggested by Rivlin and Thomas [28] and used in Tutwiler et al. [11] and Garyfallogiannis et al. [10].

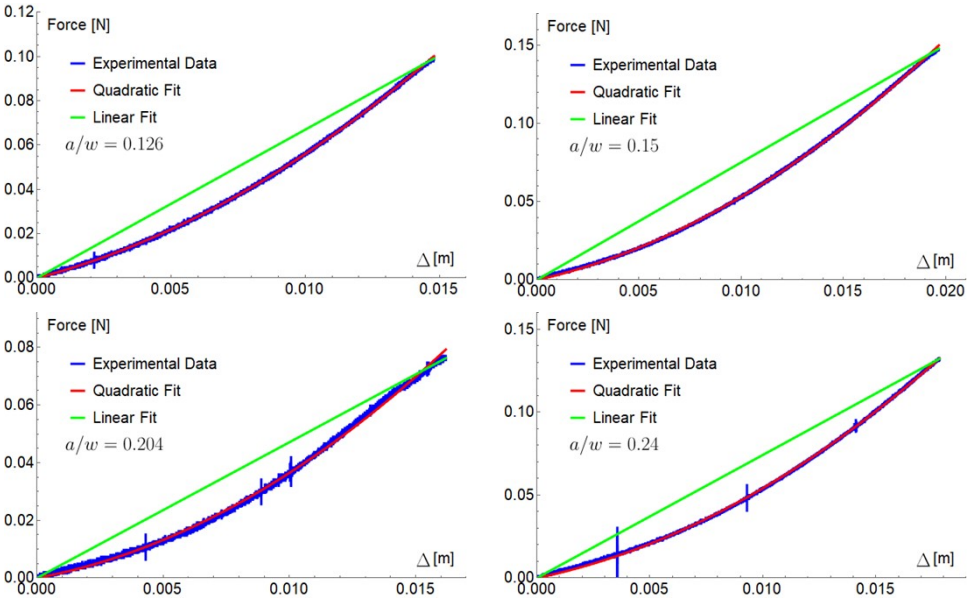

Fig. S1: Quadratic (red) vs Linear (green) fit of the experimental data (blue). The quadratic fit captures the force-displacement curve.

Comment [RI]: Fig. 5 has benn changed and no it doesn't correspond to Table S1.

Statistics of Figure 5G

θ / Region	Average (EXP)	S.D. (EXP)	Average (FEM)	S.D. (FEM)
(C)	55.5	20.5	59.2	1.8
(D)	59.7	21.0	65.5	3.2
(F)	83.6	39.9	61.9	8.8

Table S1: Average fiber angle and standard deviation with the horizontal axis as measured from confocal microscopy and predicted from FE simulations for the 3 different stretched regions in C, D, and F.

Fracture toughness dependence on fibrin(ogen) concentration

The fracture toughness $\mathcal{G}_c$ estimated from experiments in Mode II shear (this work) and Mode I tension ([10, 11]) for 2.9 and 2.7 mg/ml fibrin(ogen) concentrations are compared in Fig. S2. These two concentrations are very close and given that they correspond to two different types of experimental settings, the argument that the fracture toughness is a material parameter is further strengthened. The fracture toughness as a function of the initial fibrin(ogen) concentration/solid volume fraction ϕ_s^{ref} is shown in Fig. S3. The solid volume fraction $\phi_s^{ref} = 0.0107$ only corresponds to the Mode II shear experiments, while all the others are for the Mode I tension experiments from[10, 11]. Note that the fibrin(ogen) concentrations $1, 2.7, 2.9, 5$ and 10 mg/ml correspond to $\phi_s^{ref} = 0.0037, 0.0100, 0.0107, 0.0185$ and 0.0370, respectively (see [10] for the conversion from fibrin(ogen) concentration to solid volume fraction). Blue points are the average of the experimentally determined fracture toughness from (3) following Tutwiler et al. [11], while red points are the average toughness values for various crack lengths computed using using (5) from the FEM simulation results. i.e., J^*-integral. The corresponding standard deviation bars are also shown. The experimental estimates of fracture toughness $\mathcal{G}_c$ for tension are taken from [10] which uses a linear interpolation of the force-displacement curves. The estimates for the toughness $\mathcal{G}_c$ in shear are calculated from a quadratic interpolation of the force-displacement curves as discussed above. The FE simulation values for both shear and tension are evaluated using the constitutive model with the refitted material parameters. The FE simulation values in this figure accounts for the compressive response of the fibers which was neglected in [10]. Fig. S3 is therefore an improved and more complete version of Fig.7 in [10].

The curves are the power law fits of the form $A\left(\phi_s^{ref}\right)^n$, where A and n are the fitted parameters. Lake and Thomas [64], in a theoretical treatment of the underlying network physics, also obtained a power law dependence of the fracture toughness on the solid volume fractions for highly elastic materials. Their exponent was $n = 2/3$, whereas in our fit the exponents are higher $n = 0.78$ for $\mathcal{G}_c$ and 0.94 for G_c. The exponents are larger for gels studied here than the elastomers of Lake and Thomas [64] because diffusion of liquid through the pores dissipates energy Also, the exponents in Fig. S3 are higher than the ones in [10], since the material description in this work includes non-vanishing compressive stiffness of fibrin fibers.

The trend in the fracture toughness as a function of fibrin volume fraction is consistent, i.e., toughness increases with fibrin(ogen) concentration, excluding the 2.9 mg/ml concentration in shear. Although experiments and theory provide similar results for the energy release rate in shear, they are overall slightly less than those obtained from Mode I tension experiments. Two important factors might be responsible for this: 1) the difficulties related to configuring the experiments, the specimens are small, slippery, wet, and extremely soft materials, and 2) the crack before it propagates, is observed to blunt significantly at an angle, which brings the intense stress-strain crack tip fields closer to the boundaries of the specimen. The clamping of the specimen is known

to create intense fields at the clamped boundaries [65], which interact with the crack tip field, and lead to faster degradation of the material. This phenomenon is further exacerbated in the shear specimens used in this work, because they have smaller overall dimensions ($w = h = 20$ mm and $t = 4$ mm) than the Mode I tension specimens ($w = h = 30$ mm and t~6.5 mm).

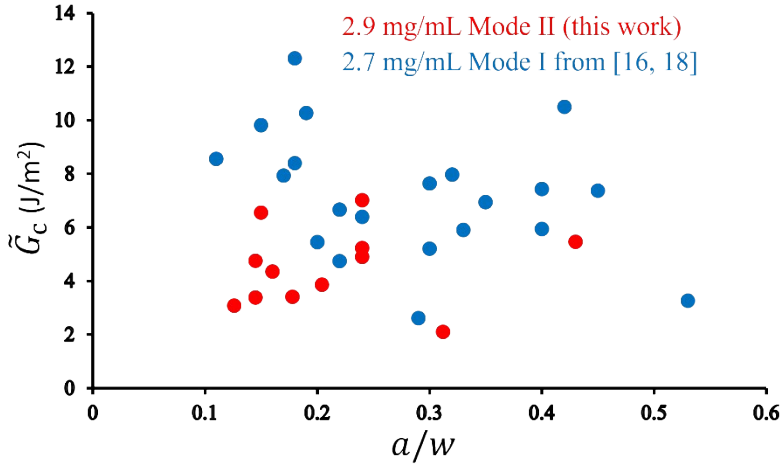

Fig S2: Comparison between $\tilde{G}_c$ values between clots under Mode I tension (adapted from [9, 10]) and clots subject to Mode II shear loading (this work).

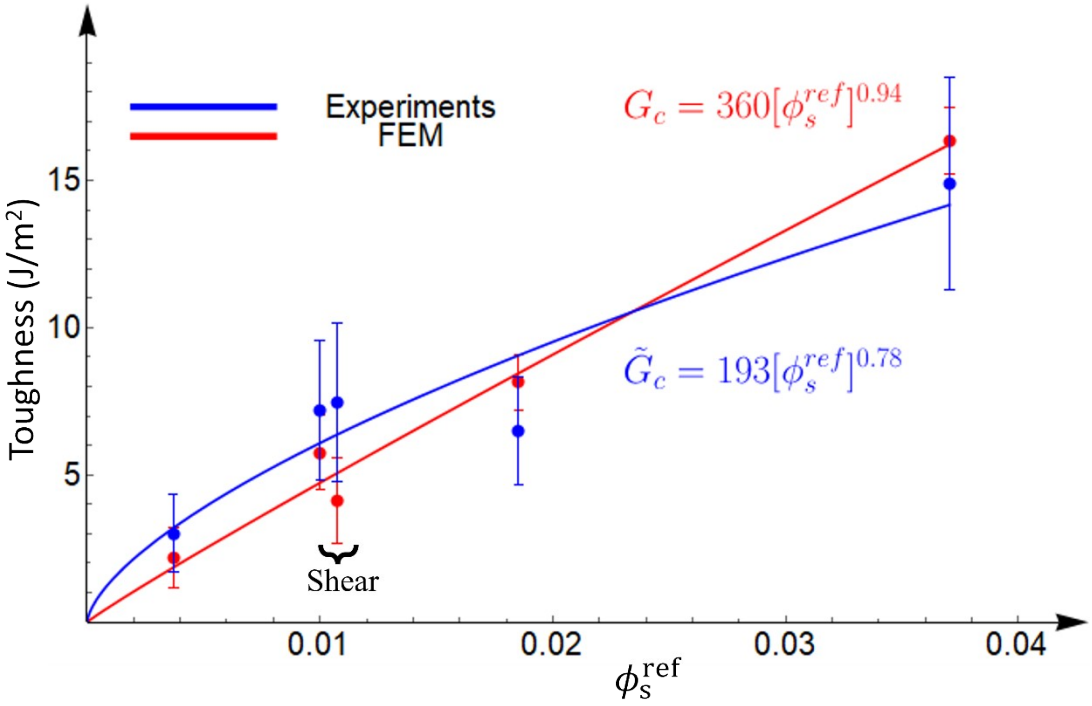

Fig. S3: Fracture toughness (critical energy release rate) and power law fits for the 5 different fibrin(ogen) concentrations/solid volume fractions ϕ_s^{ref} as predicted by experiments and FE

simulations. The solid volume fraction $\phi_s^{ref} = 0.0107$ only corresponds to the shear experiments, all the other solid volume fractions are for the Mode I tension experiments from [10, 11]. The dots are the average values for various crack lengths, and the bars correspond to $\pm$ S.D. The experimental estimates $\mathcal{G}_c$ in simple shear are based on quadratic interpolation of the force-displacement curves, while those for tension are baed on a linear interpolation. The FE simulation values of the toughness are calculated using the refitted model with the non-zero compressive stiffness of fibrin fibers. For each fibrin(ogen) concentration, we have several toughness values for different crack lengths computed with FEM using the Δ_c at peak force. The uncertainty of the FEM values is just +/- the SD of the calculated toughness values.

Stress-strain relation of a single fiber

The (nominal) stress-strain relation $g(E_p)$ is made of three different responses. Initially, the fibrin in the fibers is in a folded state for tensile strains less than the transformation strain ε_{transf} ($0 \le E_p \le \varepsilon_{transf}$). The stress increases linearly with E_p and c_f is the modulus in the folded state. Under compression ($E_p \le 0$), the fibers are assumed to have a non-vanishing stiffness unlike Tutwiler et al., [11] and Garyfallogiannis et al.,[10]. This is more realistic than the vanishing compressive stiffness assumption made in the previous works, because even after buckling the fibers can resist compression, and as compaction accumulates the fibers come in contact and the stresses rise. This compressive response is assumed to have a linear dependence on E_p for simplicity, but the associated modulus c_c is smaller than that in tension ($c_c < c_f$). If the fiber is stretched beyond the transformation strain ($\varepsilon_{transf} \le E_p$), then a phase transition takes place due to unfolding of fibrin at the molecular scales and its response is described by a worm-like chain model [31]. c_u is the corresponding modulus for the unfolded state and is related to the persistence length, and ε_{10} is a locking strain at which all segments/links of the protein are aligned. The described stress-strain behavior is given by:

$$g(E_p) = \alpha'(E_p) = \begin{cases} c_c * E_p & if \;\; E_p \le 0 \\ c_f * E_p & if \; 0 \le E_p \le \varepsilon_{transf} \\ \dfrac{c_u}{(\varepsilon_{10} - E_p)^2} + c_f * \varepsilon_{transf} - \dfrac{c_u}{(\varepsilon_{10} - \varepsilon_{transf})^2} & if \;\; \varepsilon_{transf} \le E_p \end{cases} \tag{S3}$$

This model is different from Garyfallogiannis et al., 2023 [10] in the compressive response, i.e., $g(E_p) \neq 0$ for $E_p \le 0$ instead of $g(E_p) = 0$. Therefore, the parameters must be refitted to the tensile and shear response of cracked specimens to accommodate this change. For the new set of parameters, only the shear modulus G of the neo-Hookean part and the folded modulus c_f change, while the modulus in compression c_c is half of c_f. All the other parameters remain the same. This

is not unexpected. For example, ε_{transf} or ε_{10} are related to the microstructural features of the network, which stay the same in both works. Table S2 presents the new material parameters used.

Model parameters	Values
c_f [kPa]	80 for 1 mg/ml 40 for 2.7, 2.9, 5, and 10 mg/ml
c_c[kPa]	$0.5 * c_f$
c_u [kPa]	1350
ε_{transf}	0.4
ε_{10}	5.0
κ	0.11
G [kPa]	50
π_0 [kPa]	1.0
β_1	1.02

Table S2: The 9 fitted material parameters for plasma clots. These parameters capture the froce-displacement curves for cracked specimens at all fibrin volume fractions considered.

A case-study in an idealized geometry and complex loading as might be experienced by a clot in a blood vessel

Fracture mechanics methodologies are a powerful way to understand and estimate the failure of components with complex geometries and under complex loading. Examples include calculations for aircraft components such as engine mounts and turbine blades, pressure vessels in nuclear power plants, and interconnections in multilayer electronic packages. In those examples, the component geometries and anticipated loading-conditions are known from design considerations and defects have been characterized from direct observations. For investigations of conditions leading to thrombotic embolization, in principle, imaging could be used to approximate the shape and large defects in thrombi. In addition, the problem inherently involves coupled fluid-solid computations for the blood and thrombus. Both are beyond the scope of this work. Nevertheless, to demonstrate how one can use fracture mechanics methodology to better understand and characterize embolization a case study is presented below for a highly idealized model of a clot in a vessel. Since the material model captures various aspects the deformation of cracked specimens such as the force-extension response, average fiber orientations, and angle of maximum stretch (or

crack growth) it must also capture the energetics of the fracture process. This allows for the computation of toughness values given in Tables S3.

The case study presented here utilizes the constitutive model adopted in this paper to demonstrate how the critical energy release rate, G_c, can determine whether a defect in a fibrin-rich clot within a blood vessel will propagate and ultimately cause embolization. The varying solid volume fraction in clots is taken into account. Relatively large values of the solid volume fraction are used because clots in blood vessels have undergone contraction. The modelling is a simplified/idealized version of the real conditions that might be encountered in the human body. A more realistic analysis would need to consider many different factors and aspects of the problem [45] including, but not limited to, the irregular shape of the clot, its age, consistency, elasticity of the blood vessel, presence of platelets and red blood cells (RBCs), and fluid mechanics.

An idealized situation of loading of a blood clot from the blood flow is considered in order to use the modeling procedure described in the main text to infer information about the fracture process. It is assumed that a blood clot is attached to the vessel wall as shown in Fig. S4. The Bernoulli equation for fluid flow is applicable everywhere and there is no turbulence in the flow. The clot is perfectly bonded to the blood vessels, which are assumed to be rigid, and there is no roughness in any surface. Note that rhythmic deformations of the vessel walls are not considered.

In our idealized study, the blood clots are taken to be 5 mm in length and attached to a blood vessel of inner diameter of 4 mm (the approximate diameter of a coronary artery). A horizontal, longitudinal crack of length a is considered in the clot on the midplane of the vessel as depicted in Fig. S4. The crack tip radius is assumed to be small and equal to 20 microns. Two degrees of stenosis/occlusion, two crack lengths, and four solid volume fractions (Tables S3 and S4) are simulated to highlight the contributions from each of these factors. The two occlusion degrees were chosen based on: 1) the availability of literature data to calculate shear rate and stresses for that occlusion, and 2) one moderately and one highly occluded case to showcase the trends. The importance of thrombus height and wall shear rate in determining the propensity to embolize was shown in [66]. The increase of fracture toughness with increasing fibrin volume fraction was demonstrated for whole blood clots in [14]. Experimental and computational demonstrations of how increased flow rate in vessels can lead to embolization of clots have been performed in [46, 47]. Note that the crack is placed mid-height of the blood vessel so that the distance of the crack from the upper surface exposed to blood flow (red region in Fig. S4) changes with the degree of occlusion. For 90% occlusion, the crack is further away from the blood flow than the 60% occlusion.

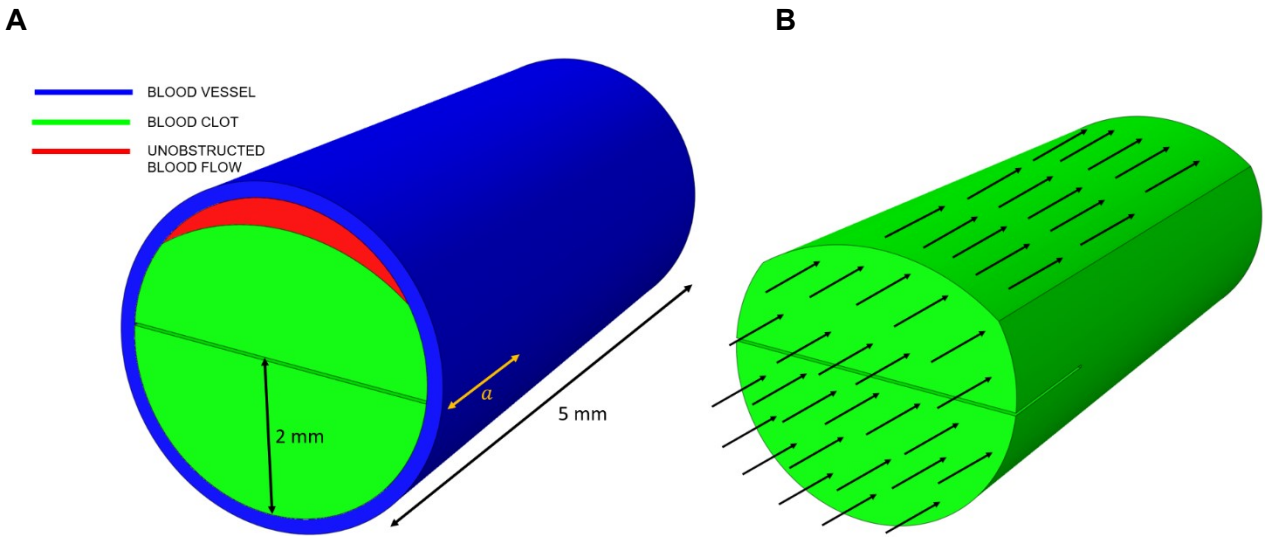

Fig. S4: Schematic representation of (**A**) the occluded vessel under consideration and (**B**) the applied traction (pressure and shear) due to the blood flow.

To focus attention on the rupture of the clot alone, the blood vessel (an artery) is assumed to be rigid. The clot is assumed to be perfectly bonded to the vessel wall, i.e. with zero displacement at the interface of the clot and vessel wall. All the other surfaces that are assumed to be exposed to blood flow are under a hydrostatic pressure of 15 kPa (~110 mm Hg), which is in the region of physiological coronary artery perfusion pressure. Furthermore, the front and top of the clot in contact with the incoming blood stream also experience a traction from the flow (Fig. S4), which is a normal pressure on the front face of the clot and shear traction on the upper face arising from the blood arterial shear rate. Following the work of Bark and Ku [48], for 60% stenosis of a coronary artery, a shear rate of 53,000 1/s is calculated to develop on the occluded vessel for a smooth surface. Strony et al. [49] calculated a shear rate of 44,000 1/s for 58% stenosis, while Siegel et al. [50] calculated 72,000 1/s for 68% stenosis. Based on these studies, we assume that for 60% occlusion the shear rate is roughly 50,000 1/s. Bark and Ku [48], conducted numerical calculations for even higher occlusion up to 98%. For 90% stenosis with a smooth surface, the shear rate is calculated to be 383,000 1/s, so we pick the value 380,000 1/s for simplicity. Assuming the blood to be a Newtonian liquid with constant viscosity of $4*10^{-3}$ Pa*s, then to approximate a well-developed flow, a shear traction of 200 Pa and 1520 Pa parallel to the blood flow is applied for 60% and 90% occlusion, respectively. The loading is applied gradually over a period of an hour in the simulations in order to suppress any rate-dependent effects from sudden loading.

The contribution from different factors is presented in Table S3. The energy release rate for each configuration is compared with a fracture toughness, i.e. the critical energy release rate for rupture, that depends on solid volume fraction, $G_c = B\left(\phi_s^{ref}\right)^n$, with $B = 260 J/m^2$ and $n = 0.85$ chosen to approximate the results obtained in Garyfallogiannis et al. [10] and this work. The values of

G_c appearing in Table S3 are for $\phi_s^{ref} \geq 0.2$ and, therefore, are extrapolations based on the above values of B and n which capture the trends in the range $0 < \phi_s^{ref} \leq 0.0307.$ Critical conditions for blood clot rupture/embolization are predicted to have been met when $J^* \geq G_c$. For 60% occluded vessels, the conditions are critical for 20% and 35% solid volume fraction, i.e., the crack propagates, but they are not critical for the higher volume fractions. For 90% occlusion, the conditions also are critical for the volume fractions of 20% and 35%. Hence, a thrombus is predicted to be more likely to rupture and released into blood flow at the earlier stages of formation, before clot contraction occurs, or when clot contraction is impaired, when the solid content is less and the material is more susceptible to deformations caused by blood shear. Note, for this highly idealized model, that the values for J^* depend weakly on the crack length, irrespective of the degree of occlusion and the solid volume fraction. Based upon this idealized model, the 60% occlusion thrombus is predicted to have a greater propensity for rupture under shear flow (higher values of J^*) than the 90% occlusion.

clot properties		a/w=0.2		a/w=0.35	
solid vol. fract.	Gc	J* for 60% occ	J* for 90% occ	J* for 60% occ	J* for 90% occ
0.2	66	191	212	200	211
0.35	107	148	125	153	120
0.5	144	128	91	132	88
0.7	192	113	67	116	66

Table S3: Energy release rate under blood flow conditions and toughness of blood clots for 60% and 90% occlusions, two crack lengths and various solid volume fractions/fibrin(ogen) concentrations. Units of both J^* and $\overline{G}_c$ are J/m^2.